CONTROL OF CHAOTIC MOTION IN ATOMIC FORCE MICROSCOPE

Kleber dos Santos Rodrigues, kleber_sr@hotmail.com
UNESP – Bauru – SP, Department of Engineering Mechanics (FEB)
Avenida Engenheiro Luiz Edmundo Carrijo Coube, 14-01
CEP: 17033-360 - Vargem Limpa - Bauru/SP
José Manuel Balthazar, josébaltha@hotmail.com
UNESP- Rio Claro, SP, Department of Statistics, Applied Mathematics and Computation(DEMAC),
Av. 24 A, N^0 1515, Bela Vista,
CEP 13506-700, Rio Claro, SP, Brazil
Angelo Marcelo Tusset, a_m_tusset@hotmail.com
UTFPR- Ponta Grossa, PR, Department of Engineering Science,
Av. Monteiro Lobato, Km 04, s/nº.
CEP: 20 - 84016-210 - Ponta Grossa-PR, Brazil
Bento Rodrigues de Pontes Júnior, brpontes@feb.unesp.br
UNESP – Bauru – SP, Department of Engineering Mechanics (FEB)
Avenida Engenheiro Luiz Edmundo Carrijo Coube, 14-01
CEP: 17033-360 - Vargem Limpa - Bauru/SP

Abstract. *This paper deals with chaotic motion in atomic force microscopy, modeling the behavior of the cantilever using partial-differential equations and using the Lennard-Jones potential to describe the interactions between the tip and the sample. The discretization of the system is achieved via Galerkin method and the dynamic of chaotic behavior is characterized by reference to phase portraits, time history, and maximum Lyapunov exponent. The method of harmonic balance is used to find a periodic solution with a periodical orbit and the stabilization of the system is achieved via State-Dependent Riccati Equation (SDRE), that drives the chaotic motion represented in the phase portrait to the periodical solution found, and the state feedback linear control method keeps the motion in the periodical orbit.*

Keywords*: Chaos, AFM, Lennard Jones Potential, SDRE Control.*

1. INTRODUCTION

Atomic Force Microscope (AFM) is a powerful tool in scanning probe microscope, its application includes manipulation of carbon nanotubes, DNA, imaging and actuation in nano-electronics, etc. (Rützel et al., 2003). In AFM, a micro-cantilever with a tip at its free end vibrates and sends a signal to a photo detector, the acquired images come from this movement and the scanning process starts.

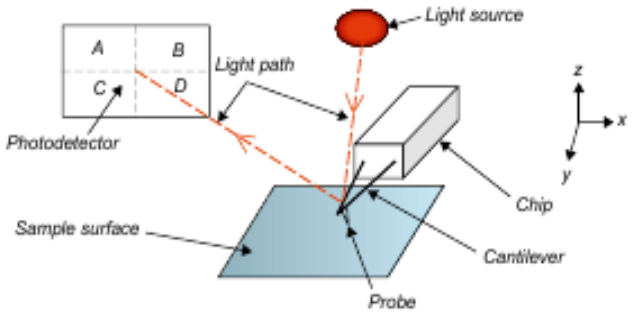

Figure 1 – Schematic of tapping mode atomic force microscope (Bowen and Hilal, (2009)).

The micro-cantilever has three modes of operation: non-contact, contact and tapping mode operation. Tapping mode is the most common type of operation, where the contact between tip and the sample may occur. To generate the images, the micro-cantilever vibrates near from its resonance. By this fact, the micro cantilever may exhibit chaotic behavior under certain circumstances. According to the literature, Sebastian et al. (2001) used a model with one-degree-of-

freedom, with linear coefficients to describe attractive and repulsive forces of the system. Garcia and San Paulo (2000) used the spring-mass equation to describe the micro-cantilever behavior, and used the theories of DMT and van der Waals forces to describe tip-sample interactions. After years, Misra and Danckowits (2007) proposed a model to represent the interactions between tip and the sample, and used event-driven method to stabilize the resonant behavior.
Chaos is a common phenomena in AFM. When this type of behavior occurs, the images are affected, what is not a desirable outcome. Mathematical modeling is commonly used to understand the behavior of the AFM micro-cantilever. Numerical simulations and analysis of the obtained figures are essential to project a control method to stabilize the system. This paper utilizes the mathematical model proposed by Rützel et al (2003) which consists of using the Bernoulli equations to describe dynamics of the micro-cantilever, and the Lennard Jones potential to describe the tip-sample interactions. In modeling process, a partial-differential equation occurs and is discretized using the method of Galerking. By using phase portrait, time history, Lyapunov exponents and Poincare maps, is possible to observe the chaotic behavior of the system. This chaotic behavior is observed in a limited interval of time, fact that interferes in the scanning process.
In general, AFM is modeled with nonlinear ordinary differential equations, those Nonlinear systems can be identified as weakly non-linear and strongly non-linear. In AFM, the weakly nonlinearities appears in non-contact mode and traditional perturbation methods like the average method and multiple scale method can be used (Nozaki et al, 2010; Aime´ et al. 1999; Boisgard et al. 1999; Nony et al. 2001; Couturier et al. 2002). Tapping mode operation is identified as a system with strong nonlinearities (Rützel, et al), by this fact, the use of those perturbation methods is a complex job. First, because analytical solutions for nonlinear system are unknown in most cases, and second, the perturbation methods are more difficult to implement (Guran, 1997).
In this paper, the method of Harmonic Balance (Nayfeh, 1995) is used to find a periodic solution. This method was choosing because it can deal with systems with strong nonlinearities. To stabilize the system and to drive it to the periodic motion, the State-Dependent Riccati equation (SDRE) control method (Fenili and Balthazar, 2010) is used and state feedback control keeps the system stabilized.
The paper is organized as follows: In section 2, the governing equations of model are obtained, by modeling the micro-cantilever behavior and modeling the interactions between the tip and the sample. Numerical simulations show the chaos in the system. In section 3, Harmonic Balance is used to find a periodic solution to the system, and SDRE and linear state feedback control methods are used to stabilize the system. The section 4 contains the conclusions about this paper and some projects to future works are mentioned.

2. THE MATHEMATICAL MODELLING

The Euler-Lagrange equation is used to describe the dynamics of the micro cantilever and Lennard-Jones potential is used to represents the interactions between the tip and the sample. L is the cantilever length, ρ is mass density, E is the Young's modulus. The area moment of inertia I of the cross-section area A is chosen in the analysis. The beam is clamped at x=0 and free at x=L. The micro cantilever deflection is $u(x,t^*)$, $\eta^* = Z - w^*(L)$ is the equilibrium gap between probe tip and sample, and the piezoelectric is modeled by $y(t^*) = Y sin\Omega t$ (Qin-Quan, Chen, 2006).

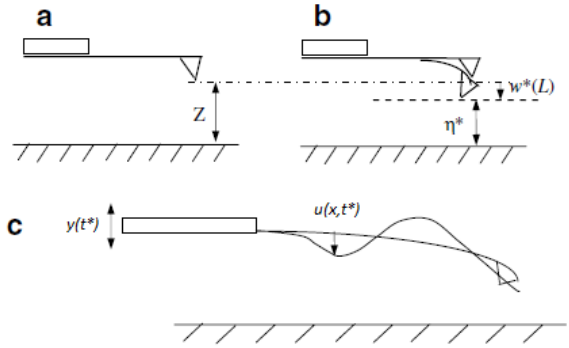

Figure 2 – A schematic of the (a) initial, (b) intermediate, and (c) current configurations associated with the micro cantilever deformation (Qin-Quan, Chen, 2006).

2.1 Modeling of cantilever deflection.

In this case is assumed that the behavior of the micro cantilever is similar with the beam behavior, than Euler–Bernoulli equation is used to describe the relationship between the beam deflection and the applied load (Witmer, 1991-1992):

$$\left(EI\frac{\partial^4 u(x,t^*)}{\partial x^4} \right) + \left(EI\frac{\partial^4 w^*(x)}{\partial x^4} \right) = q(x) \tag{1}$$

The dynamic of the beam is represented by the Euler-Lagrange beam equation:

$$S = \int_0^L \left[\frac{1}{2}\rho A\left(\frac{\partial u(x,t^*)}{\partial t^*} \right)^2 - \frac{1}{2}EI\left(\left(\frac{\partial^2 u(x,t^*)}{\partial x^2} \right)^2 + \left(\frac{\partial^2 \omega^*(x)}{\partial x^2} \right)^2 \right) + q(x)u(x,t^*) \right] dx \tag{2}$$

The first term represents the kinetic energy, the second term represents the potential energy due to internal forces and the third term represents the potential energy due to the external load. The Euler-Lagrange equation is used to determine the function that minimizes the functional *S*. For a dynamic Euler-Bernoulli beam, the Euler-Lagrange equation is

$$\frac{\partial^2}{\partial x^2}\left(EI\left(\left(\frac{\partial^2 u(x,t^*)}{\partial x^2} \right) + \left(\frac{\partial^2 \omega^*(x)}{\partial x^2} \right) \right) \right) = -\rho A\left(\frac{\partial^2 u(x,t^*)}{\partial t^{*2}} \right) + q(x) \tag{3}$$

Simplifying (3):

$$\rho A\left(\frac{\partial^2 u(x,t^*)}{\partial t^{*2}} \right) + EI\left(\left(\frac{\partial^4 u(x,t^*)}{\partial x^4} \right) + \left(\frac{\partial^4 \omega^*(x)}{\partial x^4} \right) \right) = q(x) \tag{4}$$

Where $q(x)$ represents the distributed load over the micro-cantilever length.

2.1 Boundary conditions:

Equation 4 is a fourth order partial differential equation and boundary conditions are needed to find solution $u(x,t^*)$. In this case, the load $q(x)$ is represented in a piecewise manner, load isn't a continuous function. Representation of point load as a distribution using the Dirac function in this model results:

$$\rho A\left(\frac{d^2 u(x,t^*)}{dt^{*2}} \right) + EI\left(\left(\frac{d^4 u(x,t^*)}{dx^4} \right) + \left(\frac{d^4 \omega^*(x)}{dx^4} \right) \right) = q(x)\delta(x-L)$$

With:

$$u(x,t)\big|_{x=0} = 0\,,\quad \left.\frac{du(x,t^*)}{dx}\right|_{x=0} = 0\,,\quad \left.\frac{d^2u(x,t^*)}{dx^2}\right|_{x=L} = 0$$

The partial differential equation is:

$$\rho A\ddot{u}(x,t^*) + EI(u''''+\omega^*''''(x)) = q(x)\delta\left(x-L\right) \tag{5}$$

In the next section, $q(x)$ is modeled as attraction/repulsion force derived from Lennard-Jones interaction potential (Witmer, 1991-1992):

2.2 Modeling tip surface interactions.

Lennard-Jones does not model the real contact mechanics encountered in tapping mode AFM, but it represents a generic tip-surface-interaction potential (Rützel, Lee, Raman, 2003). According to Basso *et al* (2000) and Israelachvili (1991), the representation of interaction forces between the probe tip of radius *R* and the sample surface, with a gap *z* is:

$$U_{L,J} = \frac{A_1 R}{1260 z^7} - \frac{A_2 R}{6z} \qquad P_{L,J}(z) = -\frac{\partial U_{L,J}}{\partial z} = +\frac{A_1 R}{180 z^8} - \frac{A_2 R}{6z^2}$$

Where A_1 and A_2 are the Hamaker constants, and represents repulsive and attractive potentials respectively. The Hamaker constants are given by $A_1 = \pi^2\rho_1\rho_2 c_1$ and, $A_2 = \pi^2\rho_1\rho_2 c_2$.The gap z is represented with $z = \eta^* - u(L,t^*) - Y\sin(\Omega t^*)$, than the Lennard-Jones potential is:

$$P_{L,J} = -\frac{A_1 R}{180(\eta^* - u(L,t^*) - Y\sin(\Omega t^*))^8} + \frac{A_2 R}{6(\eta^* - u(L,t^*) - Y\sin(\Omega t^*))^2} \tag{6}$$

Finally, using equation 6 in equation 5, and substitution of $q(x)$ by $P_{L,J}$, is possible to obtain the governing equation of the system:

$$\rho A\ddot{u}(x,t^*) + EI(u''''(x,t^*) + \omega^*''''(x)) = \qquad = \left(-\frac{A_1 R}{180(\eta^* - u(L,t^*) - Y\sin\Omega t^*)^8} + \frac{A_2 R}{6(\eta^* - u(L,t^*) - Y\sin\Omega t^*)^2} \right).$$

$$.\delta(x-L) + \rho A\Omega^2 Y\sin\Omega t^* \tag{7}$$

Discretization

Next consider the situation when the excitation frequency Ω is close to the lowest frequency of the micro-cantilever. Under near-resonant forcing, and in the absence of additional internal resonances, only one mode of the micro cantilever is assumed to participate in the response (Qin-Quan and Chen, 2007):

$$u(x,t^*) = \phi_1(x) q_1(t^*) \tag{8}$$

Where $\phi_1(x)$ is the first approximate eigenfunction. Substitution of (8) into (7), multiplication of (7) by $\phi_1(x)$, subsequent integration over the domain, and the introduction of a modal damping consistent with the Q factors listed in table table1 (appendix 2) yields the single-degree-of-freedom model:

$$\ddot{y} = -d_1\dot{y} - y + B_1 + \frac{C_{11}}{(1-y-\eta sin\Omega t)^8} + \frac{C_{12}}{(1-y-\eta sin\Omega t)^2} + \eta\Omega^2 E_1 sin\Omega t \tag{9}$$

Where

$$y = \frac{x_1(t^*)}{\eta^*},\ x_1(t^*) = \phi_1(L) q_1(t^*),\ \eta^* = Z - w^*(L),\ t^* = \omega_0 t,\ d_1 = \frac{c_1}{\omega_0 \rho A \int_0^L \phi_1^2 dx},\ B_1 = (1-\bar{\alpha})\Gamma_1,$$

$$C_{11} = -\frac{A_1 R}{180k(\eta^*)^9}\Gamma_1, \qquad C_{12} = -\frac{A_2 R}{6k(\eta^*)^3}\Gamma_1,\ \omega_0^1 = \frac{EI\int_0^L \phi_1\phi_1'''' dx}{\rho A\int_0^L \phi_1^2 dx},\ \bar{\alpha} = \frac{Z}{\eta^*},\ k = \frac{3EI}{L^3},\ \eta = \frac{Y}{\eta^*},$$

$$\Gamma_1 = \frac{k\phi_1^2(L)}{\omega_0^2 \rho A\int_0^L \phi_1^2 dx},\ \bar{\Omega} = \frac{\Omega}{\omega_0},\qquad E_1 = \frac{\phi_1(L)\int_0^L \phi_1 dx}{\int_0^L \phi_1^2 dx},$$

A positive y is the micro cantilever tip displacement towards the sample, nondimensionalized by the equilibrium gap between the tip and the sample, C_{11}, C_{12}, d_1 and E_1, are non-dimensional parameters acquired by the Si-Si system under consideration. In this case, η is the vibration amplitude of the dither piezoelectric actuator nondimensionalized by the equilibrium gap width.

Table 1 - Properties and dimensions of the micro cantilevers (Rützel, Lee and Raman, (2006)).

Descriptions	*symbol*	*Si–Si(111) case*	*Si–polystyrene case*
length	*L*	449 μm	154 μm
width	*b*	46 μm	13.7 μm
thickness	*h*	1.7 μm	6.9 μm
tip radius	*R*	150 *nm*	20 *nm*
material density	ρ	2 330 $kg\ m^{-3}$	2 330 $kg\ m^{-3}$
static stiffness	*k*	0.11 $N\ m^{-1}$	40 N m^{-1}
elastic modulus	*E*	176 *GPa*	130 *GPa*
1st resonance	f_1	11.804 *kHz*	350.0 *kHz*
Q factor (air)	*Q*	100	100
Hamaker (att.)	A_2	$1.865 \times 10^{-19} J$	$1.15072 \times 10^{-19}\ J$
Hamaker (rep.)	A_1	$1\ 1.359\ 6 \times 10^{-70}\ J\ m^6$	$0.838\ 873 \times 10^{-70}\ J\ m^6$

A positive *y* is the micro-cantilever tip displacement towards the sample, nondimensionalized by the equilibrium gap between the tip and the sample. *Y* is the vibration amplitude of the dither piezoelectric actuator nondimensionalized by the equilibrium gap width.
Writing equation (10) in state space forma and considering the following substitutions: $x_1 = y$, $x_2 = \dot{y}$. The differential equation (9) can also be represented in state space:

$$\begin{aligned} \dot{x}_1 &= x_2 \\ \dot{x}_2 &= -x_1 - d_1 x_2 + B_1 + \frac{C_{11} + C_{12}(1 - x_1 - \eta\sin(\bar{\Omega}t))^6}{(1 - x_1 - \eta\sin(\bar{\Omega}t))^8} + \eta\bar{\Omega}^2 E_1 \sin(\Omega t) \end{aligned} \tag{10}$$

2.3 System with chaotic behavior

Numerical simulations with (10) using software Matlab, integrator ODE45, step length h=0.001, parameters; $d_1 = 0.01, B_1 = -0.148967, C_{11} = -4.59118\times10^{-5}, E_1 = 1.57367$, $C_{12} = 0.149013$, η=0.9 and $\bar{\Omega} = 1$, with initial conditions $x(0) = 0.2$ and $\dot{x}(0) = 0$ follows:

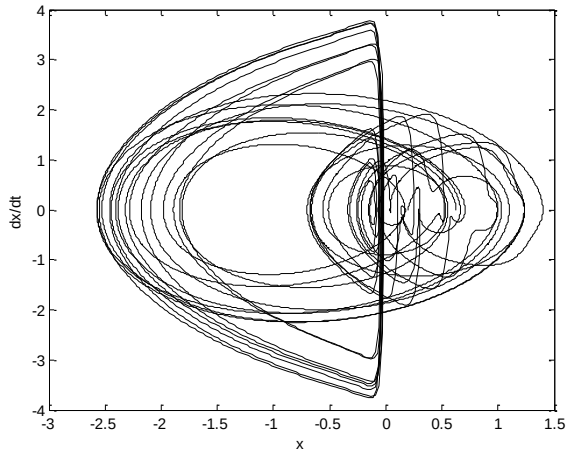

Figure 3 – Phase portrait of chaotic behavior.

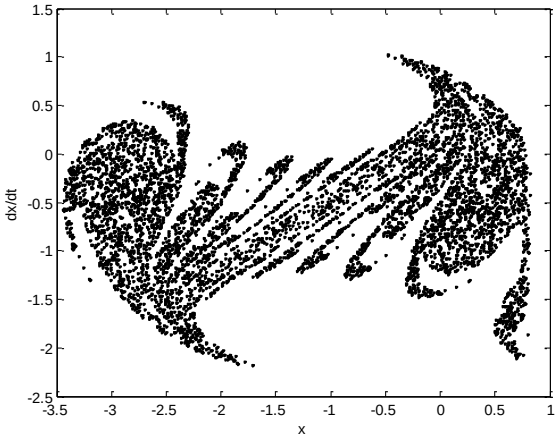

Figure 5 – Poincare maps with strange attractor.

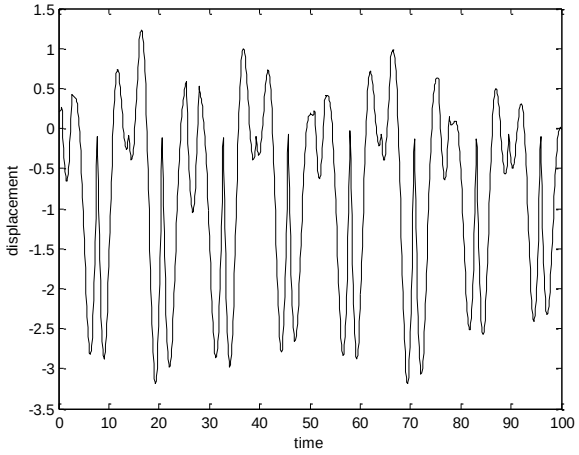

Figure 4 – Time history of chaotic behavior.

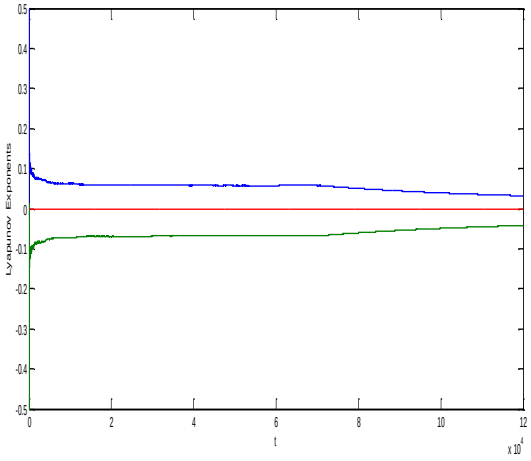

Figure 6 – Lyapunov exponents with positive

In figures 3 and 4, irregular behavior is detected. In figure 5, Poincare maps show strange attractors and in figure 6, with $t = 1.2\times10^5$, Lyapunov exponents obtained the follow results: $\lambda_1 = 0.010154$, $\lambda_2 = -0.020146$, $\lambda_3 = 0$. In fact, is possible to observe that chaotic behavior occurs in the studied interval of time.

3. THE CONTROL METHOD

The SDRE nonlinear regulator produces a closed-loop solution, which is locally asymptotically stable (see details on: (Mracek and Cloutier, 1998; Banks et al., 2007). We remarked that the procedure for drive the tip position to a desired point or trajectory, via SDRE technique, considers successive optimal solutions for static equations and stabilize the system by the feedback control (Shawky et al., 2007). The goal is to use the control U, so that the response of the controlled system is a periodic and asymptotically stable orbit. Next, the periodic desired orbit is obtained via Harmonic Balance method.

3.1.Harmonic Balance method

The main idea of the method is to consider a periodic solution of (9) in the following form (Nayfeh, 1995):

$$y = A_0 + A_1\cos(\omega t) + B_1 sen(\omega t) + A_2\cos(2\omega t) + B_2 sen(2\omega t) + ... \tag{11}$$

Next, consider (11):

$$y = A_0 + A_1\cos(t) + B_1 sen(t) \tag{12}$$

Considering initial conditions $y(0) = y_0$ and $\dot{y}(0) = \dot{y}_0$, follows:

With $y(0) = y_0$,

$$A_0 + A_1 = y_0 \tag{13}$$

and $\dot{y}(0) = \dot{y}_0$

$$B_1 = \dot{y}_0 \tag{14}$$

Considering (13) and (14) and substituting the expansion (12) in (9), then equating coefficients of constant terms equal to zero, the terms of $\cos(\omega t)$ and $\sin(\omega t)$ equal to zero too, we find the following constants terms:

$$A_0 + B_1 = 0 \tag{15}$$

Considering (12), (13) and (14) with the initial conditions: $y(0) = 0.2$ e $\dot{y}(0) = 0$ is obtained:

$$y = -0.148967 + 0.348967\cos(t) \tag{16}$$

Next, in figure 7, is possible to observe the periodical orbit represented by equation 16, this orbit is a possible solution of system represented by the equation 9:

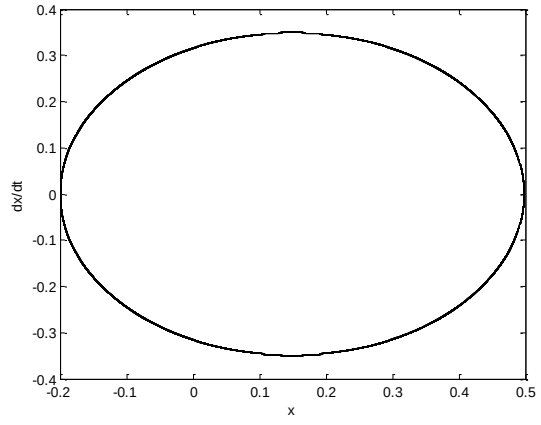

Figure 7 – Periodic orbit obtained by the Harmonic Balance

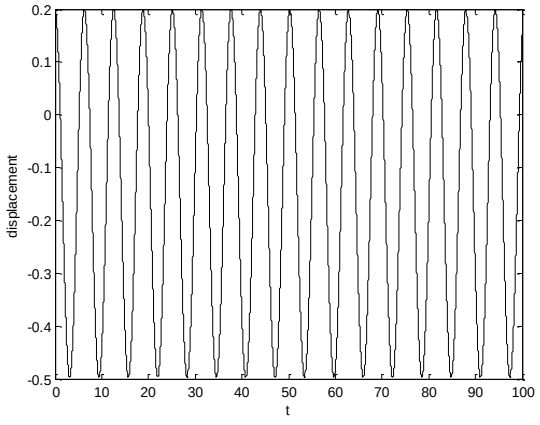

Figure 8 – Time history periodical solution

3.2. Application of proposed control method

The control proposed in this paper follows the principle of using two controls. The feedfoward control in order to maintain the system (10) in desired orbits (16) and state feedback control to bring the system to the desired orbit. Considering the nonlinear system (10) represented as follows:

$$\dot{x} = A(x)x + F \tag{17}$$

Where $x \in R^n$ is the state vector, $A \in R^{n \times n}$ is a dependent state matrix, F is the nonlinear vector of terms not state dependent.
With control, the system (10) is:

$$\dot{x} = A(x)x + F + U \tag{18}$$

With:

$$U = u_f + u \tag{19}$$

u_f is the feedfoward control:
By using $x(0) = x_0$, and substituting (19) in (18), the system (18) can be represented by:

$$\dot{x} = A(x)x + Bu \tag{20}$$

Where: $B \in R^{nxm}$ is a constant matrix, and u is the state feedback linear control. The state feedback linear control u can be found by using the State-Dependent Riccati Equation Method (SDRE).
Writing the dynamical system defined by (10) in the form of (18):

$$\begin{aligned} \dot{x}_1 &= x_2 \\ \dot{x}_2 &= -x_1 - d_1 x_2 + F \end{aligned} \tag{21}$$

where:

$$F = B_1 + \frac{C_{11} + C_{12}(1 - x_1 - \eta \sin(\bar{\Omega}t))^6}{(1 - x_1 - \eta \sin(\bar{\Omega}t))^8} + \eta \bar{\Omega}^2 E_1 \sin(\bar{\Omega}t) \tag{22}$$

Introducing control (19), in system (21), follows that (Shawky et al.,2007):

$$\begin{bmatrix} \dot{x}_1 \\ \dot{x}_2 \end{bmatrix} = \begin{bmatrix} 0 & 1 \\ -1 & -d_1 \end{bmatrix} \begin{bmatrix} x_1 \\ x_2 \end{bmatrix} + \begin{bmatrix} 0 \\ 1 \end{bmatrix} u \tag{23}$$

The system in the form (24) implies that the origin is an equilibrium point, a condition which allows apply the SDRE control to achieve the control u (Shawky et al., 2007).
The matrices A and B are represented by:

$$A = \begin{bmatrix} 0 & 1 \\ -1 & -d_1 \end{bmatrix}, \; B = \begin{bmatrix} 0 \\ 1 \end{bmatrix} \tag{24}$$

The state feedback control is obtained from:

$$u = -R^{-1}(x)B^T(x)P(x) = -K(x)e \tag{25}$$

with: $e = (x - x^*)$, x^* represents the desired orbit (16) and $P(x)$ is the State-Dependent Riccati Equation solution:

$$P(x)A(x)+A^T(x)P(x)-P(x)B(x)R^{-1}(x)B^T(x)P(x)+Q(x)=0 \tag{26}$$

defining:

$$Q=\begin{bmatrix}10^3 & 0\\ 0 & 10^3\end{bmatrix},\ R=\begin{bmatrix}10^{-5}\end{bmatrix}$$

The cost functional to be minimized through the SDRE control is given by:

$$J=\int_0^\infty (e^T Q(e)e+u_r{}^T R(u)u_r)dt \tag{27}$$

Next, in Figure 8 can be observed efficiency of the proposed control system to bring the chaotic behavior to the desired orbit (16), in Figure 9 can be observed the phase portrait considering the application of the control (18) in (10).

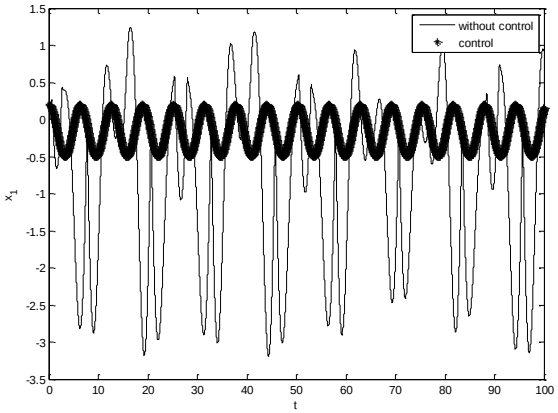

Figure 9 - Comparison between not controlled and controlled system

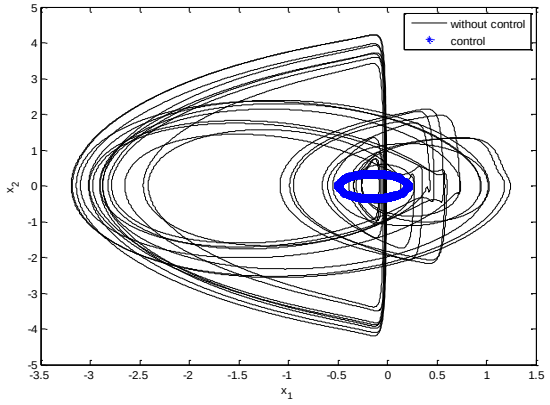

Figure 10 – Phase portrait of both systems, not controlled and controlled system

As can be seen in figures 9 and 10, is possible to observe that the proposed control was effective and with easy implementation. The simulations also shows that the error between the desired orbit and the obtained obit, by using the control matrices Q and R, was $\max|x-x^*|=0.000015$ for $t\le 100$. Is important to note that the error be reduced by adjusting the weighting matrices Q and R in LQR control used, and is possible to affirm the controlled system is globally stable.

4. CONCLUSIONS

The method of Harmonic Balance (Nayfeh, 1995) was successfully applied in the system and a periodic orbit was found (fig. 7 and 8), the SDRE control method was easily implemented, and was possible to drive the chaotic behavior to the periodic one. Finally state feedback linear control kept the system stabilized with small error.
As seen in this paper, chaos in the system was detected in a limited interval of time, there are no guarantees that chaotic behavior occurs when $t\to\infty$, but even in a limited interval of time, chaos prejudices the obtaining of images. The presence of chaos can lead to errors while imaging samples using dynamic AFM are achieved, thereby introducing an element of deterministic uncertainty in nanometrology (Hu and Haman, 2006). In future papers, basins of attraction and bifurcation diagrams will be used to a deeper analysis of the system that represents the tapping mode Atomic Force Microscopy model.

5. ACKNOWLEDGMENTS

Authors thank CNPq and Fapesp for financial support. K.S. Rodrigues thanks CAPES for fellowship support.

6. REFERENCES

Aime´, J. P., Boisgard, R., Nony, L. & Couturier, G. 1999 Nonlinear dynamic behavior of an oscillating tip–micro lever system and contrast at the atomic scale. Phys. Rev. Lett. 82, 3388–3391.

Basso, M., Giarre, L., Dahleh, M. & Mezic, I., 2000, " Complex dynamics in a harmonically excited Lennard-Jones oscillator: micro-cantilever sample interaction in scanning probe microscopes." J. Dynam. Syst. Meas. Control 122, 240–245.

Boisgard, R., Michel, D. & Aim´e, J. P. 1999 Hysteresis generated by attractive interaction: oscillating behavior of a vibrating tip–micro-cantilever system near a surface. Surf. Sci. 401, 199–205

Couturier, G., Nony, L., Boisgrad, R. & Aim´e, J.-P. 2002 Stability of an oscillating tip in noncontact atomic force microscopy: theoretical and numerical investigations. J. Appl. Phys. 91, 2537–2543

Dankowicks H. ,Zhao X. 2006 Characterization of intermittent contact in tapping mode force microscopy;. J. Comput. Nonlinear Dynam. - April 2006 - Volume 1, Issue 2, 109

Fenili, A, Balthazar, J.M., 2011, "The rigid-flexible nonlinear robotic manipulator: Modeling and Control.", Communications in Nonlinear Science and Numerical Simulation, 16, Issue 5, 2332-2341

Garcia R. and San Paulo A., 2000, "Dynamics of a vibrating tip near or in intermittent contact with a surface." Physical Review B 61, 20.

Guran, A, 1997, "Nonlinear Dynamics: The Richard Rand 50th anniversary volume", World scientific publishing, Co Pte Ltda, Series on stability, vibration and control of systems. Series B: Vol 2 -24,25.

Hu, S., Haman A., (2006), "Chaos inatomic force microscopy", Birckand NCN Publications. Paper 39. http://docs.lib.Purdue. edu/nanopub/39.

Israelachvili, J., 1991, "Intermolecular and surface forces", 2nd edn. Academic.

Mracek C.P., and Cloutier J.R., (1998), "Control designs for the nonlinear benchmark problem via the state-dependent Riccati equation method." International Journal of Robust and Nonlinear Control, 8, 401-433.

Misra S., Dankowicks H., Paul M.R., 2007, "Event-driven feedback tracking and control of tapping-mode atomic force microscopy". First Cite Publishing.

Nony, L., Boisgrad, R. & Aim´e, J.-P. 2001 Stability criterions of an oscillating tip-cantilever system in dynamic force microscopy. Eur. Phys. J. B 24, 221–229.

Nozaki R., Pontes Jr B.R, Tusset A. M., Balthazar J.M., 2010, "Optimal linear control to an atomic force microscope: (AFM) problem with chaotic behavior", Dincon'10, 9th Brazilian conference on dynamics, control and their Applications

Nozaki R., Balthazar J.M., Pontes Jr. B.R., 2011, "Nonlinear dynamics, chaos and control in Atomic Force Microscope" master degree dissertation, FEB, UNESP.

Qin-Quan H., Chen L., 2007, "Bifurcation and chaos in atomic force microscope." Elsevier, Chaos, Solutions and Fractals 33, 711–715, 2006.

Rutzel S., Lee S.I., Raman A., 2003, "Nonlinear dynamics of atomic-force-microscope probes driven in Lennard-Jones potentials." Proc R Soc London A ; 459:1925–48.

Sebastian A., Salapaka M. V., Chen D. J., and Cleveland J. P., 2001, "Harmonic and power balance tools for tapping mode atomic force microscope", Journal of Applied Physics, 89**,** pp. 6473–6480.

Shawky, A. M.; Ordys, A. W.; Petropoulakis, L.; Grimble, M. J. "Position control of flexible manipulator using non-linear with state-dependent Riccati equation". Proc. IMechE, 221 Part I: J. Systems and Control Engineering, 475-486, 2007.

Witmer E.A., (1991-1992). "Elementary Bernoulli-Euler Beam Theory". *MIT Unified Engineering Course Notes*. pp. 5-114 to 5-164

7. RESPONSIBILITY NOTICE

The authors are the only responsible for the printed material included in this paper.